

Investigation of Fuel Cell Materials and Liquid Water Transport by Means of Synchrotron Imaging

H. Markötter^a, J. Haußmann^b, R. Alink^c, K. Dittmann^a, C. Tötze^{a,d}, P. Krüger^{b,*}, M. Klages^b, T. Arlt^a, B. Müller^c, H. Riesemeier^c, J. Scholta^b, D. Gerteisen^c, I. Manke^a, J. Banhart^{a,d}

^a Helmholtz-Zentrum Berlin, 14109 Berlin, Germany

^b Zentrum für Sonnenenergie und Wasserstoff-Forschung Baden-Württemberg, 89081 Ulm, Germany

^c Fraunhofer Institut für Solare Energiesysteme, 79110 Freiburg, Germany

^d Technische Universität Berlin, 10623 Berlin, Germany

^e Bundesanstalt für Materialforschung und -prüfung, 12205 Berlin, Germany

* present address: CONSULECTRA Unternehmensberatung GmbH, 22083 Hamburg, Germany

Synchrotron imaging allows addressing various important issues in fuel cell research, for example water distribution and transport. The water distribution in polymer electrolyte membrane fuel cells (PEMFCs) was observed quasi in-situ directly after operation by means of synchrotron tomography. The 3D data set was compared with the tomogram of a dry cell in order to separate the water distribution from cell materials. Engineered transport pathways realized by perforating holes through the gas diffusion layer (GDL) are a recent approach to optimize water transport and cell performance. For some parameter sets a cell performance increase and an improvement of stabilization have already been proven. We present high resolution investigations of the water distribution in perforated GDLs of operating PEMFCs by means of in-situ synchrotron radiography. The surrounding areas of the holes exhibited a distinct hydrophilic character.

Introduction

Polymer electrolyte membrane fuel cells (PEMFCs) are considered as the most promising fuel cell types for future applications in the automotive industry or in stationary power supply systems (1-6). As a product of the electrochemical reaction of hydrogen and oxygen liquid water is formed in the cell. This needs to be transported to the outlets of the cell because flooding of the gas diffusion layer (GDL) reduces power output due to gas supply blockage by liquid water agglomerations (7). On the contrary a dry membrane has to be avoided as well, as the membrane will take damage, which reduces the cell lifetime. Altogether, water management plays a crucial role and broad access to the water distribution is a prerequisite for successful optimization of the water management (8-13).

In the recent years synchrotron radiography have been successfully applied for in-situ investigations on the water distribution in the GDL (14-30).

Quasi in-situ fuel cell synchrotron tomography was applied to visualize the cell structure three-dimensionally and to provide a real-time image of the water agglomerations in the cell (31, 32).

The second part of the article deals with in-situ measurements of a perforated GDL. Perforating the GDL is a straight-forward approach to optimize the water management by introducing drainage holes. A cell performance increase was shown by Gerteisen et al. (6) for a GDL that was laser perforated in through plane direction. We present radiographic study of the dynamic water transport processes in the fuel cell during startup (33).

Fuel Cells

Fuel cells for tomography

Quasi in-situ fuel cell tomography was performed on a dedicated test cell designed by the ZSW (Zentrum für Sonnenenergie und Wasserstoff-Forschung Baden-Württemberg in Ulm, Germany) to obtain the three dimensional water distribution (31, 34). The test cell was designed to meet the instrumental requirements: Within the tomographed section the cell width was adopted to fit into the field of view (see figure 1). Within this section the metallic end plates were replaced by poly carbonate in order to realize higher beam transmission and to increase the detection sensitivity to liquid water. During the tomographic acquisition gas flows were shut off and temperature was reduced from 50° C to 25° C in order to conserve the present water distribution within the cell. Furthermore, the supply tubes were removed and the connections sealed in order to prevent water evaporation. In this way the water distribution was captured in all three dimensions. Within the imaged area these cells were 14 mm wide and equipped with commercially available GDLs of the types SGL 10BC and SGL 25BC, respectively. The flow field geometry was formed by single meander shaped channels, which were 500 µm wide and deep separated by 500 µm wide ribs. The fuel cells were operated at current densities between 40 and 1000 mA/cm².

Fuel cells for radiography

The radiographic study of a perforated GDL was performed using fuel cells with an active area of 100 × 100 mm². To allow for sufficient beam transmission through the imaged cell sections holes with a diameter of 10 mm were drilled into the end plates and the current collector plates. For the measurements presented in figure 4 a Toray TGP-H-090 GDL was used, which corresponds to the GDL used by Gerteisen et al. in (6). The flow fields were made of three-fold meander shaped channels which were 800 µm wide.

Imaging Setup

The measurements were performed at the HZB tomography station at the BAMline at the synchrotron facility BESSY II in Berlin (35). The tomography setup is sketched in figure 1. The cell was mounted on a rotation table and rotated stepwise during tomography. The cell was projected onto a CdWO₄ scintillator, which was then imaged via a mirror onto the 4008 × 2672 pixel CCD array. A tomographic scan contained more

than 1000 projections covering an angular range of 180°. A double multilayer monochromator provided a monochromatic beam with an energy resolution of $\Delta E/E < 1.5\%$. An energy of 15 keV was chosen yielding an optimum relation between transmission through the cell and sensitivity to liquid water. Spatial resolutions of 5 - 12 μm were achieved for the present test cells with pixel sizes of 2.2 μm for radiography and 4.8 μm for tomography. The field of view was $8.8 \times 5.9\text{ mm}$ during radiography and $19.2 \times 10\text{ mm}$ during tomography. The time interval between two projections was 7 s, whereas a whole tomographic acquisition took around 60 minutes.

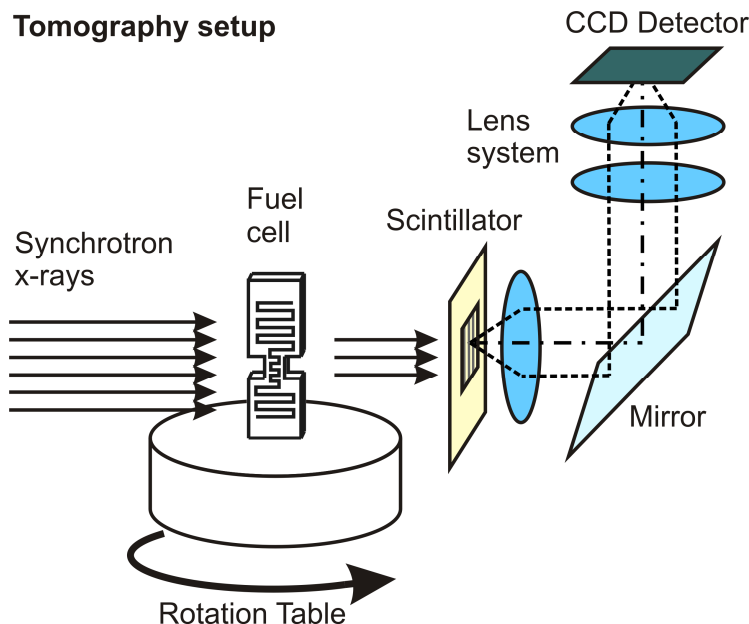


Figure 1: Tomography setup. A radiographic image of the fuel cell is projected onto a scintillator, which is then imaged with a CCD detector via a mirror.

Results

Tomography of fuel cells

Figure 2 shows a cutout of a tomogram of a fuel cell. The left part of the cell as well as the flow field back planes were virtually cut away to allow for a view through the flow field channels onto the SGL 25BC GDL and the inner components such as membrane and catalyst layer. This three-dimensional dataset can be cut in any direction at any position.

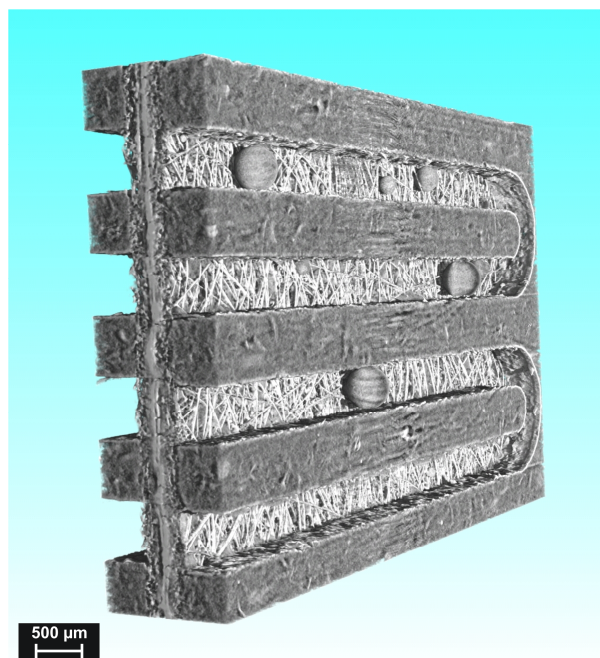


Figure 2: Cutout of a reconstructed fuel cell. Clearly visible are water droplets on the GDL in the single meander flow field channel.

For a more detailed analysis of liquid water in the GDL it is beneficial to distinguish between GDL fibers and smallest water agglomerations. Therefore, the fuel cell was also tomographed in a dry state. Subtracting the datasets of the dry and the water containing cells yields the liquid water distribution only. However, the tomograms must be perfectly matched for this purpose. This is realized by adjusting the exact position of the datasets in three dimensions as well as the exact rotation in three dimensions. Due to cell operation changes of the local fuel cells structure can occur, e.g. membrane thickness changes (31). This causes detectable deformations of the GDL so that some fibers were not totally removed in the calculated water distribution. Also high absorbing materials such as the catalyst cause artifacts in the result (see membrane in figure 3). To reduce artifacts produced by membrane swelling prior to the tomographic acquisition the cell was purged with humidified hydrogen without drawing current. This way a membrane hydration state similar to that during cell operation was realized while the remaining cell components stay free of liquid water. However, in most cases sufficiently precise matching of the tomograms could only be adjusted for restricted cell sections. In figure 3 vertically and horizontally aligned cuts are shown separately for anode as well as cathode side.

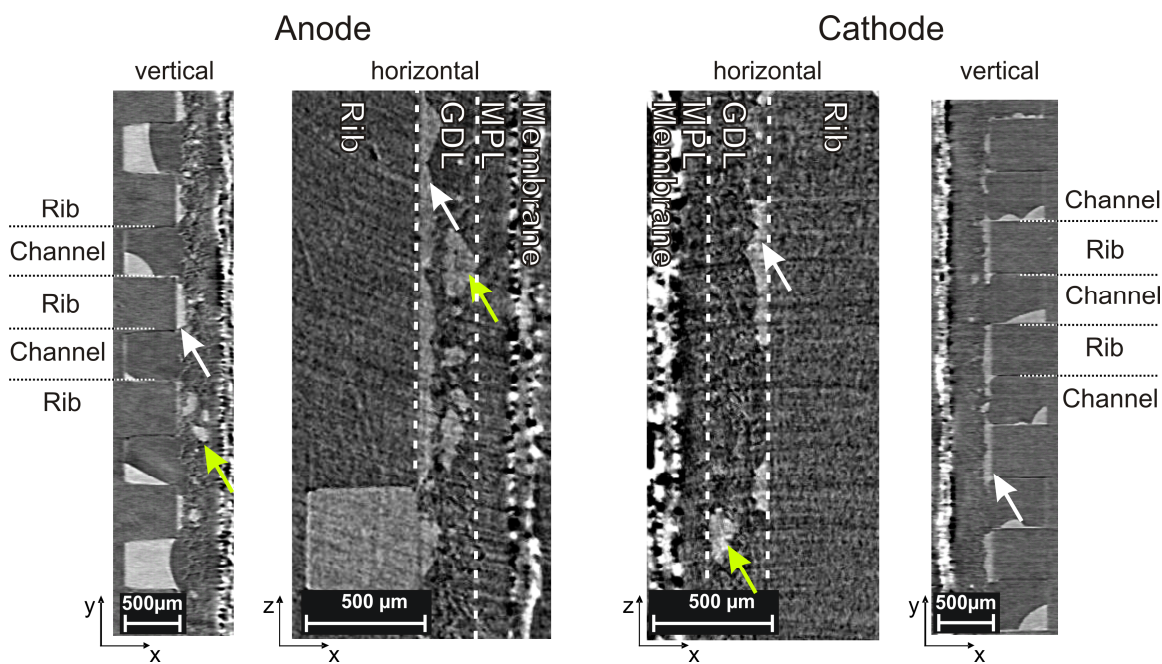


Figure 3: Vertical and horizontal cuts through a cell. For easier identification of the water distribution inside the gas diffusion layer (SGL 10BC) the cell materials were subtracted. Water is found in the GDL at the rib of the flow field (white arrows) as well as far inside the GDL (green arrows).

The influence of gravity appears in the vertical cuts as most droplets in the channels agglomerate on the bottom. The horizontal cuts are shown at a higher magnification and it can be seen that water is distributed throughout the whole GDL volume (see arrows in figure 3). However, most agglomerations are sited directly at the ribs of the flow field (white arrows in figure 3). These areas are less affected by the supply gas stream and water is preferably accumulating there.

Radiography of perforated gas diffusion layers

A straight forward approach is the realization of drainage holes that are intended to transport the liquid water efficiently from catalyst through GDL into the channel. The previously found performance gain of Gerteisen et al. (6) have not been fully understood yet and the visualization of the water distribution promise further insights into the underlying processes in and around the perforation holes. Radiographic imaging was applied for the investigation of dynamic processes. Images taken during cell operation were normalized with an image of the dry cell before operation. The attenuation of the synchrotron beam by liquid water is described by the Beer-Lambert law. The inverse calculation delivers the transmitted water depth d for each pixel:

$$d = \ln(I / I_0) / -\mu(E) \quad [1]$$

Where $\mu(E)$ is the attenuation coefficient of water at the used photon energy, I the transmission at that pixel during cell operation and I_0 the transmission through a dry cell. The water distribution is observed in through plane direction during startup at a current density of 500 mA/cm². In figure 4 the temporal evolution of liquid water at a selected perforation hole is shown. Figure 4a gives a rough sketch of the horizontally aligned

channel as well as the position of the perforation hole. During the first minutes of operation small water droplets were found at the channel walls, see figure 4b. After 7 min 21 s the boundary of the perforation hole was covered with water and the shape of the hole became visible. 10 minutes after startup the hole itself filled up within 2 minutes with liquid water (Figure 4e-f) and stayed flooded until the end of the measuring time of 25 minutes. It was found that the surrounding area in the GDL was constantly filling with water before it entered the hole. For all perforations the vicinity of the holes was filling up with liquid water, but not all holes were filled. This indicates a more hydrophilic character of the GDL fibers within the vicinity of the hole, which was already postulated by Alink et al. (36). They assumed an oxygenation which was most probably caused by heat during the perforation process, which is realized with a ND:YAG laser.

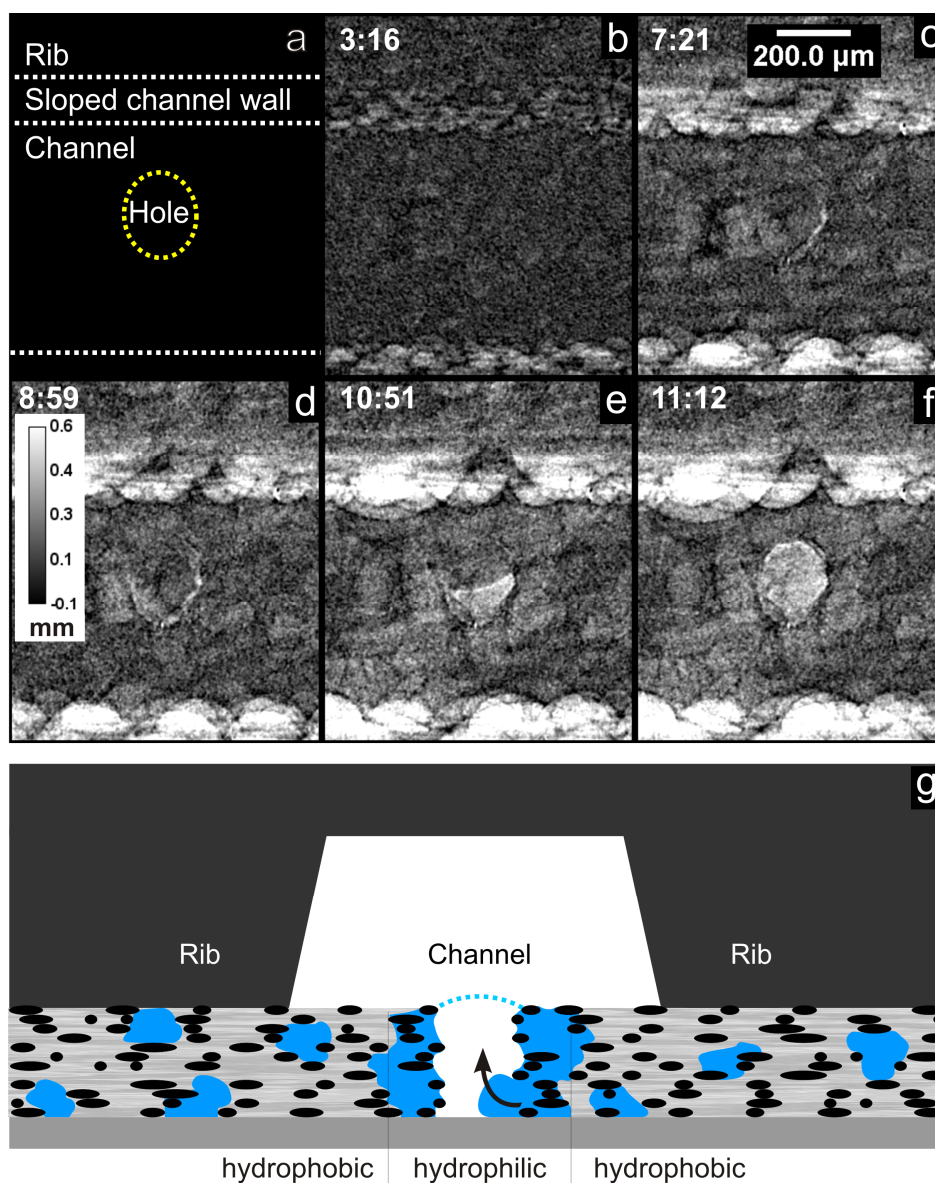


Figure 4: Water distribution at a laser cut drainage hole through Toray TGP-H-090 at cathode side. The surrounding as well as the perforation hole itself was filling up with liquid water. (partly modified from (33))

Conclusions

The liquid water distribution in the GDL of PEMFCs was investigated three dimensionally by means of quasi in-situ synchrotron tomography. Most of the water agglomerations were sited right at the ribs of the flow field structure. These areas are less affected by the supply gas stream. There, evaporation is less intense than in the GDL sections located at a channel. A transport into the channels seems unlikely, as the position at the rib represents a dead end in through plane direction.

Furthermore, a perforated Toray TGP-H-090 GDL was visualized by dynamic radiography. The observation of the liquid water evolution during startup of the fuel cell showed a filling of the perforation hole and a more hydrophilic behaviour of the nearby vicinity of the GDL. That area is continuously filling up with liquid water and staying filled until the end of the measurement.

References

1. W. Vielstich, A. Lamm and H. A. Gasteiger, *Handbook of Fuel Cells – Fundamentals, Technology and Applications*, John Wiley & Sons, Chichester (2003).
2. L. Carrette, K. A. Friedrich and U. Stimming, *Fuel Cells*, **1**, 5 (2001).
3. C.-Y. Wang, *Chem Rev*, **104**, 4727 (2004).
4. J. Garche, C. K. Dyer, P. T. Moseley, Z. Ogumi, D. A. J. Rand and B. Scrosati, *Encyclopedia of Electrochemical Power Sources*, p. 4538, Elsevier, Amsterdam (2009).
5. B. C. H. Steele and A. Heinzel, *Nature*, **414**, 345 (2001).
6. D. Gerteisen, T. Heilmann and C. Ziegler, *J Power Sources*, **177**, 348 (2008).
7. S. Ohyagi, T. Matsuda, Y. Iseki, T. Sasaki and C. Kaito, *J Power Sources*, **196**, 3743 (2011).
8. S. Litster, D. Sinton and N. Djilali, *J Power Sources*, **154**, 95 (2006).
9. P. Berg, K. Promislow, J. S. Pierre, J. Stumper and B. Wetton, *J Electrochem Soc*, **151**, A341 (2004).
10. C. Ziegler, H. M. Yu and J. O. Schumacher, *J Electrochem Soc*, **152**, A1555 (2005).
11. G. Lin, W. He and T. V. Nguyen, *J Electrochem Soc*, **151**, A1999 (2004).
12. U. Pasaogullari and C.-Y. Wang, *J Electrochem Soc*, **152**, A380 (2005).
13. A. Bazylak, D. Sinton and N. Djilali, *J Power Sources*, **176**, 240 (2008).
14. I. Manke, H. Markötter, C. Tötze, N. Kardjilov, R. Grothausmann, M. Dawson, S. Haas, D. Thomas, A. Hoell, C. Genzel, C. Hartnig and J. Banhart, *Adv Eng Mater*, **13**, 712 (2011).
15. I. Manke, C. Hartnig, M. Grünerbel, W. Lehnert, N. Kardjilov, A. Haibel, A. Hilger, J. Banhart and H. Riesemeier, *Appl Phys Lett*, **90**, 174105 (2007).
16. C. Hartnig, I. Manke, R. Kuhn, N. Kardjilov, J. Banhart and W. Lehnert, *Appl Phys Lett*, **92**, 134106 (2008).
17. I. Manke, C. Hartnig, N. Kardjilov, H. Riesemeier, J. Goebbels, R. Kuhn, P. Krüger and J. Banhart, *Fuel Cells*, **10**, 26 (2010).
18. C. Hartnig, I. Manke, J. Schloesser, P. Krüger, R. Kuhn, H. Riesemeier, K. Wippermann and J. Banhart, *Electrochem Commun*, **11**, 1559 (2009).

19. H. Markötter, Manke I., Hartnig Ch., Krüger Ph., Wippermann K., Arlt T., Choinka G., Riesemeier H., Banhart J., *MP Materialprüfung - Materials Testing*, **52**, 698 (2010).
20. T. Sasabe, P. Deevanhxay, S. Tsushima and S. Hirai, *Electrochem Commun*, **13**, 638 (2011).
21. T. Sasabe, S. Tsushima and S. Hirai, *International Journal of Hydrogen Energy*, **35**, 11119 (2010).
22. R. J. Bellows, M. Y. Lin, M. Arif, A. K. Thompson and D. Jacobson, *J Electrochem Soc*, **146**, 1099 (1999).
23. J. Owejan, T. Trabold, D. Jacobson, D. Baker, D. Hussey and M. Arif, *International Journal of Heat and Mass Transfer*, **49**, 4721 (2006).
24. M. A. Hickner, N. P. Siegel, K. S. Chen, D. S. Hussey, D. L. Jacobson and M. Arif, *J Electrochem Soc*, **155**, 427 (2008).
25. D. Kramer, J. Zhang, R. Shimoi, E. Lehmann, A. Wokaun, K. Shinohara and G. G. Scherer, *Electrochim Acta*, **50**, 2603 (2005).
26. P. Boillat, D. Kramer, B. C. Seyfang, G. Frei, E. Lehmann, G. G. Scherer, A. Wokaun, Y. Ichikawa, Y. Tasaki and K. Shinohara, *Electrochem Commun*, **10**, 546 (2008).
27. C. Hartnig, I. Manke, N. Kardjilov, A. Hilger, M. Grünerbel, J. Kaczerowski, J. Banhart and W. Lehnert, *J Power Sources*, **176**, 452 (2008).
28. A. Schröder, K. Wippermann, W. Lehnert, D. Stolten, T. Sanders, T. Baumhöfer, N. Kardjilov, A. Hilger, J. Banhart and I. Manke, *J Power Sources*, **195**, 4765 (2010).
29. C. Tötze, I. Manke, T. Arlt, H. Markötter, N. Kardjilov, A. Hilger, S. H. Williams, P. Krüger, R. Kuhn, C. Hartnig, J. Scholta and J. Banhart, *Nucl. Instrum. Methods Phys. Res. Sect. A-Accel. Spectrom. Dect. Assoc. Equip.*, **663**, 48 (2012).
30. W. Maier, T. Arlt, C. Wannek, I. Manke, H. Riesemeier, P. Krüger, J. Scholta, W. Lehnert, J. Banhart and D. Stolten, *Electrochem Commun*, **12**, 1436 (2010).
31. P. Krüger, H. Markötter, J. Haussmann, M. Klages, T. Arlt, J. Banhart, C. Hartnig, I. Manke and J. Scholta, *Journal of PowerSources*, **196**, 5250 (2011).
32. I. Manke, C. Hartnig, M. Grünerbel, J. Kaczerowski, W. Lehnert, N. Kardjilov, A. Hilger, J. Banhart, W. Treimer and M. Strobl, *Appl Phys Lett*, **90**, 184101 (2007).
33. H. Markötter, R. Alink, J. Haußmann, K. Dittmann, T. Arlt, F. Wieder, C. Tötze, M. Klages, C. Reiter, H. Riesemeier, J. Scholta, D. Gerteisen, J. Banhart and I. Manke, *International Journal of Hydrogen Energy*, **37**, 7757 (2012).
34. H. Markötter, I. Manke, P. Krüger, T. Arlt, J. Haussmann, M. Klages, H. Riesemeier, C. Hartnig, J. Scholta and J. Banhart, *Electrochem Commun*, **13**, 1001 (2011).
35. W. Görner, M. P. Hentschel, B. R. Müller, H. Riesemeier, M. Krumrey, G. Ulm, W. Diete, U. Klein and R. Frahm, *Nuclear Instruments and Methods in Physics Research Section A: Accelerators, Spectrometers, Detectors and Associated Equipment*, **467-468**, 703 (2001).
36. R. Alink, D. Gerteisen and W. Mérida, *Fuel Cells*, **11**, 481 (2011).